

Composite Floor Systems under Column Loss: Collapse Resistance and Tie Force Requirements

Joseph A. Main, Ph.D., A.M.ASCE¹

Abstract: This paper presents a computational assessment of the performance of steel gravity framing systems with single-plate shear connections and composite floor slabs under column loss scenarios. The computational assessment uses a reduced modeling approach, while comparisons with detailed model results are presented to establish confidence in the reduced models. The reduced modeling approach enables large multi-bay systems to be analyzed much more efficiently than the detailed modeling approaches used in previous studies. Both quasi-static and sudden column loss scenarios are considered, and an energy-based approximate procedure for analysis of sudden column loss is adopted, after verification through comparisons with direct dynamic analyses, further enhancing the efficiency of the reduced modeling approach. Reduced models are used to investigate the influence of factors such as span length, slab continuity, and the mode of connection failure on the collapse resistance of gravity frame systems. The adequacy of current structural integrity requirements is also assessed, and based on the computational results, a new relationship is proposed between the uniform load intensity and the tie forces required for collapse prevention.

CE Database subject headings: Buildings; Connections; Composite materials; Finite element method; Floors; Nonlinear analysis; Progressive collapse; Steel structures.

¹ Research Structural Engineer, Engineering Laboratory, National Institute of Standards and Technology, Gaithersburg, MD 20899-8611, joseph.main@nist.gov

Introduction

From the early 1980s (ANSI 1982) to the present (ASCE 2010), standards for structural design in the United States have included requirements for “general structural integrity.” Such requirements are intended to ensure that structures are resistant to disproportionate collapse, in which local damage spreads progressively, resulting in a partial or total collapse that is disproportionate to the initiating event. ASCE 7-10 (ASCE 2010) includes “extraordinary event” load combinations, to be used in assessing residual capacity following the notional removal of selected load-bearing elements. While ASCE 7-10 does not include specific provisions or criteria for resistance to disproportionate collapse, the 2009 version of the International Building Code (IBC) (ICC 2009, Section 1614) introduced structural integrity requirements for design of high-rise buildings in occupancy categories III and IV. These new requirements include minimum levels of tensile strength for the end connections of beams in steel frame structures.

For U.S. military buildings, the Unified Facilities Criteria (UFC) 4-023-03 (DOD 2009) provides tie force requirements that were developed with the specific objective of preventing collapse under internal and exterior column loss scenarios (Stevens 2008). In the development of these tie force requirements (Stevens 2008), it was noted that most steel connections are not capable of sustaining the magnitudes of rotation necessary to carry the gravity loads through catenary action (i.e., through tensile forces in the beams). For this reason, the 2009 version of the UFC 4-023-03 requires that tie forces be carried by the floor system, unless the connections can be shown capable of developing the required tensile forces while sustaining substantial rotations of 0.20 rad. This approach contrasts sharply with the integrity requirements in the 2009 IBC, which specify minimum tensile capacities for the end connections of beams without consideration of the rotational capacity of the connections.

Recent full-scale tests (Lew et al. 2012) and computational studies (Main et al. 2010, Alashker et al. 2011, Sadek et al. 2012) have demonstrated the good performance of seismically designed steel moment connections under column loss, with the connections sustaining rotations almost twice as large as those observed in previous seismic tests and developing significant vertical capacity through a

combination of flexural and catenary action. In contrast, analyses of composite floor systems with simple shear connections (Foley et al. 2008, Sadek et al. 2008, Alashker et al. 2010) have suggested a susceptibility to collapse under column loss. While Sadek et al. (2008) found that the composite floor slab significantly enhanced the capacity of a 2 bay \times 2 bay floor system relative to the capacity of the bare steel framing system, the capacity of the composite system was still inadequate to sustain the gravity loads under sudden loss of the center column. Alashker et al. (2010) considered the influence of a number of factors on the collapse resistance of the 2 bay \times 2 bay system, including thickness of the steel deck, area of the welded wire reinforcement, and the number of bolts in the shear tab connections.

Motivated by these concerns about the susceptibility to collapse of steel gravity framing systems with composite floors, this paper presents a reduced modeling approach for these systems and uses this approach to investigate the influence of factors such as span length, slab continuity, slab reinforcement, and the mode of connection failure on the capacity of the systems. The reduced modeling approach enables large multi-bay systems to be analyzed much more efficiently than the detailed approach used previously by Sadek et al. (2008) and Alashker et al. (2010). A number of previous studies have proposed reduced modeling approaches to represent the anisotropic, nonlinear behavior of concrete slab on profiled steel deck. Kwasniewski (2010) used alternating strips of shell elements to represent a composite floor slab with steel deck. Alashker et al. (2011) proposed an approach in which lines of beam elements parallel to the ribs were used to represent the steel deck, while the concrete slab was modeled with shell elements. Alashker and El-Tawil (2011) proposed a design-oriented model to represent the collapse resistance of composite floors. Cashell et al. (2011b) analyzed composite slabs using simplified analytical modeling as well as finite element modeling with an orthotropic shell element formulation, also presenting comparisons with experimental measurements reported by Cashell et al. (2011a).

This study, like Kwasniewski (2010), uses alternating strips of shell elements to represent the anisotropic behavior of the composite slab. However, while Kwasniewski (2010) incorporated integration points representing the steel deck in both types of alternating strips, the proposed approach includes the

steel deck only in strips representing the ribs, conservatively neglecting the stiffness and strength of the metal deck in the across-rib direction. In addition, while the strips of shell elements proposed by Kwasniewski (2010) were of the same width as the ribs of the steel deck, it was found in this study that strips much wider than the rib width can be used in order to enhance computational efficiency, without significant loss in accuracy. An energy-based approximate procedure for analysis of sudden column loss (Powell 2003, Guo and Gilsanz 2003, Izzuddin et al. 2008) is also applied and verified in this study, enabling the structural capacity under sudden column loss to be evaluated using the results of a single quasi-static pushdown analysis. Analyses are performed using explicit time integration in LS-DYNA (Hallquist 2007), and comparisons of detailed and reduced model results are presented to establish confidence in the reduced models. The reduced modeling approach is then used to (1) evaluate the collapse resistance of composite floor systems from prototype buildings, (2) assess the effectiveness of the structural integrity requirements in the 2009 IBC (ICC 2009) and the tie force requirements in UFC 4-023-03 (DOD 2009) in preventing collapse under column loss scenarios, and (3) evaluate the tie force levels required for prevention of collapse.

Prototype Composite Floor Systems

Fig. 1 shows the plan layouts of two composite floor systems considered in this paper, which represent portions of the interior gravity framing systems of two prototype 10-story buildings described in Main and Sadek (2012). The alternate plan layouts shown in Fig. 1 were developed to examine the influence of span length on disproportionate collapse resistance. Since the focus of this study is on the collapse resistance of gravity frame systems, no moment frames are considered. Beams and girders in the prototype gravity frames were designed assuming fully composite action with the concrete slab, while it is noted that partially composite beams are common in practice. ASTM A992 structural steel beams and columns are connected using single-plate shear connections, illustrated in Fig. 2. Shear connections on the east-west beams in building B have four bolts, while all other shear connections have three bolts. The

composite floor slab consists of 83 mm of lightweight concrete (specific weight = 17.3 kN/m³, nominal compressive strength = 20.7 MPa) over a 20 gage steel deck (ASTM A653, Grade 33) with a depth of 76 mm and an average rib width of 152 mm. The concrete slab has welded wire reinforcement (ASTM A82 steel wire), with W1.4 wire (cross-sectional area = 9.0 mm²) in a 152 mm × 152 mm grid spacing. AWS D1.1 type B shear connector studs (AWS 2010) with a diameter of 19 mm are used to develop composite action between the steel beams and the concrete slab. Circled columns in Fig. 1 indicate column loss scenarios considered subsequently. While the tie force requirements in UFC 4-023-03 were developed to prevent collapse under both interior and exterior column loss scenarios (Stevens 2008), only interior column loss scenarios are considered in this paper. Exterior column loss scenarios for these prototype floor systems are considered in Main and Sadek (2012).

Gravity Loads

ASCE 7-10 (ASCE 2010, Section 2.5.2.2) specifies a load combination for assessing residual capacity of structural systems following the notional removal of load-bearing elements. For the floor systems considered in this study, this load combination can be simplified as follows:

$$1.2D + 0.5L \quad (1)$$

in which the factor 1.2 is selected for the dead load, rather than 0.9, because gravity loads do not stabilize the structural system. Roof live loads, snow loads, and rain loads are omitted because a typical intermediate floor of the structure is considered. For a typical floor in the prototype buildings, the total dead load D is 3.64 kN/m², which includes the floor self-weight of 2.2 kN/m² and a superimposed dead load of 1.44 kN/m². The nominal live load of 2.40 kN/m², applicable to offices, is reduced using Eq. (4.7-1) in ASCE 7-10, based on the influence area of a typical floor beam, yielding a combined gravity load, $1.2D + 0.5L_{\text{office}}$, equal to 5.40 kN/m² for building A and 5.36 kN/m² for building B.

In some of the analyses presented subsequently, the floor systems are unable to sustain the combined floor loading from Eq. (1) under sudden column loss. In such cases, it is of interest to compare

the capacity of the floor systems with the expected (or “point-in-time”) value of the gravity loading. This lower level of gravity loading is given as follows:

$$1.05D + L_{\text{survey}} \quad (2)$$

where $L_{\text{survey}} = 0.52 \text{ kN/m}^2$ denotes the mean live load for offices based on survey data, from Table C4-2 of ASCE 7-10 (ASCE 2010). The dead load factor in Eq. (2) is taken as 1.05 in order to more accurately represent the expected dead load, because the mean dead load in modern construction typically exceeds the nominally specified value by 5 % to 10 % (Ellingwood et al. 2007, p. 22). The total gravity loading given by Eq. (2) equals 4.34 kN/m^2 for both buildings A and B.

Reduced Modeling of Composite Floor Systems

Fig. 3 shows a reduced model of a 2 bay \times 2 bay portion of the floor system from prototype building A, in which the wide flange girders, beams, and columns are represented using beam elements, and the composite floor slab is represented using shell elements. The columns extend one story above and below the floor slab, and the tops and bottoms of the columns are modeled as pinned, except for the center column, which is unsupported vertically. This 2 bay \times 2 bay floor system was previously studied by Sadek et al. (2008) and Alashker et al. (2010) using a detailed model, and comparisons of detailed and reduced model results are presented subsequently.

Composite Floor Slab

As illustrated in Fig. 3, the concrete slab on steel deck is represented in the reduced model using alternating strips of shell elements denoted “strong” and “weak” strips, which are oriented parallel to the ribs in the steel deck. As illustrated in Fig. 4, the weak strips include only the concrete above the top of the steel deck, while the strong strips include the full depth of concrete. No contribution from the steel deck is included in the weak strips, in order to represent the much lower stiffness and strength of the steel deck across the ribs than along the ribs. Six integration points are used through the thickness of each shell

element, with four integration points representing the concrete, a fifth integration point representing the welded wire, and a sixth integration point representing either the steel deck (for the strong strips) or a “dummy material” with negligible stiffness and strength (for the weak strips). The strips of shell elements used in this study have a width of 610 mm, which is about four times the average rib width. Results in Main and Sadek (2012) show that further refinement of the mesh produces little change in the computed results. Main and Sadek (2012) considered two arrangements for the alternating strips, in which either (a) the weak strips or (b) the strong strips were located along the girders. This comparison showed that placing the weak strips along the girders is preferable, as in Fig. 3, enabling the use of larger shell elements for the floor slab without sacrificing accuracy. While elements larger than 610 mm could potentially be used to speed up the computations, this element size was selected to achieve a good spatial resolution of the in-plane membrane forces for subsequent plotting and analysis.

The thickness of the steel deck used in the strong strips is scaled to represent the steel area of only the bottom segment of each rib [e.g., for the deck profile in Fig. 4, the bottom segment of each rib has a width of 132 mm, while the average rib width is 152 mm, so the actual deck thickness of $t_d = 0.91$ mm is scaled by the ratio $(132 \text{ mm}) / (152 \text{ mm})$]. Assuming that forces develop only in the bottom segment of each rib results in lower stiffness and strength than if the entire steel deck were engaged. However, this is consistent with the observation based on detailed modeling by Alashker and El-Tawil (2011) that since the deck is attached to the beams by shear studs, only a portion of the deck effectively yields at peak load. While the area of concrete above and below the top surface of the deck is correctly represented by the alternating strips in Fig. 4(b), the tapered profile of the concrete in the ribs is represented by applying weighting factors to the corresponding integration points in the strong strips.

Integration points through the thickness of the floor slab are assigned distinct material models for the concrete, welded wire reinforcement, and steel deck. The concrete in the floor slab is modeled using equations and material data from Eurocode 2, part 1.2 (material 172 in LS-DYNA), which represent concrete cracking in tension and crushing in compression. The minimum specified compressive strength

of 20.7 MPa is used in the model, and this compressive strength is reached at a strain of 0.25 %, beyond which the stress decreases linearly to zero at a compressive strain of 2 %. A tensile strength of 2.07 MPa is used in the model, and cracking is activated when the maximum in-plane principal stress reaches this value. After cracking, the tensile stress decreases following a bilinear curve, reaching zero stress at a tensile strain of 0.25 %. The welded wire reinforcement and the steel deck are represented using a piecewise linear plasticity model (material type 24 in LS-DYNA), with minimum specified yield and ultimate strength values of 450 MPa and 515 MPa, respectively, for the A82 steel wire, and 230 MPa and 310 MPa, respectively, for the A653 Grade 33 steel deck. The wire reinforcement is modeled as continuous, under the assumption that splices are sufficient to develop the full capacity of the wire.

Fracture is modeled using element erosion, in which shell elements are deleted when all integration points have reached or exceeded their specified values of plastic strain at fracture. Plastic strains at fracture were calibrated to match specified values of elongation under uniaxial tension. The minimum specified elongation of 20 % at fracture is used for the A653 Grade 33 steel deck. Because ASTM standard A82 (ASTM 2007) does not specify a minimum elongation for welded wire reinforcement, a value of 5 % was used for the fracture elongation, based on tensile test data reported by Gilbert and Sakka (2007), which indicated an elongation between 4 % and 6 % at fracture. For elongations beyond 5 %, no resistance is provided at integration points representing the wire reinforcement, although element erosion does not occur until all integration points have reached their applicable fracture strain. For the strong strips of shell elements (see Fig. 4), element erosion is specified at an elongation of 20 %, corresponding to fracture of the steel deck. The resistance of the weak strips becomes negligible at a much smaller engineering strain of 5 %, after failure of the wire reinforcement. However, retaining such failed elements in the analysis has little effect on the solution. For convenience in post-processing, element erosion for the weak strips is specified at a larger engineering strain of 38 %, corresponding to the strain at which the steel deck would be completely flat, after unfolding of the ribs. Analysis results were found to be insensitive to changes in the erosion strain specified for the weak strips.

Shear Stud Connectors

As illustrated in Fig. 5, rigid links extend vertically from the centerline of the beams and girders to the top-of-steel elevation, and elements representing shear studs connect these rigid links to nodes of the shell elements representing the floor slab. Using a discrete beam formulation (beam element formulation 6 in LS-DYNA with material type 119), the force vs. slip curve labeled “reduced model” in Fig. 6 is used to represent the shear behavior of the shear studs along both the longitudinal and transverse axes of the beam or girder. Transverse forces in the shear studs can be generated by membrane forces in the floor slab under large displacements. The initial portion of the piecewise-linear “reduced model” curve in Fig. 6 approximates the empirical load-slip relationship proposed by Ollgaard et al. (1971) based on pushout testing of shear studs without steel deck. The empirical curve is also plotted in Fig. 6, and while the curve is plotted up to a slip of 25 mm, it is noted that the equation is only intended to represent the initial load-slip behavior, up to slip of about 5 mm. Based on observations at larger slip values by Rambo-Roddenberry (2002, pp. 71, 114), for shear studs welded through steel deck, the shear force in the reduced model curve remains constant at the ultimate load between 5 mm and 15 mm, after which it drops linearly to zero at a displacement of 25 mm. AWS D1.1 Type B studs (AWS 2010) are assumed, with an ultimate strength of 450 MPa, and the ultimate shear strength of a 19 mm diameter shear stud was calculated as $Q_u = 76.1$ kN based on the AISC Specification (AISC 2010, Section I8.2a). Elastic flexural stiffness is also specified for the shear stud elements to provide torsional restraint along the top flange of the floor beams. The number of shear stud elements along each beam in the model depends on the mesh size selected and is generally less than the number specified in the design. To provide the proper shear resistance in the model, force values in the force vs. slip curve (Fig. 6) are scaled by the ratio of the actual number of shear studs to the number of shear stud elements in the model.

Single-Plate Shear Connections

The primary components of the reduced connection model in Fig. 5 are the bolt springs, which represent the in-plane behavior of the connection, and which are interconnected with rigid links to maintain the proper connection geometry. Following the approach outlined by Main and Sadek (2013), each bolt spring is implemented using a zero-length discrete beam element, with distinct load-deformation curves to represent yielding and failure (1) along the beam axis and (2) in vertical shear. Failure is represented by deleting each bolt spring from the model when its resistance drops to zero along either axis. The yield and ultimate capacities of the bolt springs are calculated using equations in the AISC Specification (AISC 2010) with a resistance factor of $\phi = 1$. Minimum specified values of yield strength F_y and ultimate strength F_u for each type of steel are used in these equations, and connection capacities are divided by the number of bolts to obtain the capacity of a single bolt row. Connection deformations at yield and at the ultimate load are calculated using equations in Sadek et al. (2008), based on data from seismic testing (FEMA 2000). Sadek et al. (2008) considered axial behavior controlled by bolt tear-out and proposed a load-deformation relationship of the form labeled “gradual softening” in Fig. 7, which exhibits a gradual drop in resistance after the ultimate load in tension is reached and no drop in resistance after the ultimate load in compression is reached. In this study an alternate form of load-deformation relationship is also considered, labeled “sudden fracture” in Fig. 7, which exhibits a steeper drop in resistance after the ultimate load is reached in both tension and compression, reflecting failures that have been observed experimentally (Thompson 2009, Weigand et al. 2012).

Because of the three-dimensional nature of composite floor systems, membrane forces in the floor slab can subject the connections to a combination of torsion and transverse shear. Accordingly, an additional discrete beam element (labeled “shear tab” in Fig. 5) is used to represent the torsional and transverse shear behavior of the shear tab connection. Using this “shear tab” beam element, piecewise-linear relationships based on detailed model results (see Main and Sadek 2012, section 4.3.2) are specified for the torsional and transverse shear behavior of the connections, while the in-plane axial, shear, and

bending behavior is represented by the bolt springs. Each individual bolt spring provides no resistance to rotation, but bending moment in the connection is generated through differential axial forces that develop in the bolt springs under in-plane rotation. A “gap spring” is included at the level of the bottom flange of the beam, to allow bearing forces to be transmitted if the initial gap between the beam flange and the column closes (see Fig. 2). Concrete contact springs could be included to represent bearing of the concrete slab against the columns, using properties defined in Sadek et al. (2008). However, these springs were found to have a negligible effect for column removal scenarios considered in this study and therefore were not included in the analyses.

Detailed Modeling of Composite Floor Systems

Fig. 8 shows portions of a detailed model of the 2 bay \times 2 bay floor system shown in Fig. 3, based on the model developed by Sadek et al. (2008). Only one quarter of the floor system is modeled, with appropriate boundary conditions on the planes of symmetry. Concrete in the floor slab is represented using solid elements, while the welded wire reinforcement is represented using beam elements sharing common nodes with the solid elements (i.e., no bond slip). The profiled steel deck and the wide flange steel sections are represented using shell elements. The typical edge length of the elements is about 38 mm. Contact is defined among the various components of the model to prevent interpenetration. Shear studs are represented using beam elements sharing common nodes with the solid and shell elements of the concrete slab and steel deck, while a spot weld model (material type 100 in LS-DYNA) is used to represent the portion of the shear stud connecting the steel deck to the beam flange, with a shear failure criterion based on the nominal shear strength from the AISC Specification (AISC 2010, Section I8.2a). While the detailed model is based on that developed by Sadek et al. (2008), several changes were made for the analyses in this study, as summarized in the following points:

- **Connections:** While Sadek et al. (2008) used specially calibrated shell elements to model the in-plane behavior of the shear tab connections, the detailed model in this study uses the same bolt spring

elements as in the reduced model. As illustrated in Fig. 8(b), these bolt springs interconnect nodes of shell elements on the beam webs with nodes of shell elements representing the shear tabs. Two rows of shell elements represent each shear tab, and since bearing-induced deformations and failure are incorporated in the bolt springs, shell elements in the row connected to the bolt springs are assigned an elastic material model to preclude plastic deformations. Shell elements in the row connected to the column are assigned a piecewise linear plasticity material model, to capture yielding of the connections when subjected to torsion and transverse shear loading.

- **Steel modeling:** As in Sadek et al. (2008), the steel components in the detailed model are represented using piecewise linear plasticity models, and fracture is modeled using element erosion. However, the detailed model in this study uses values of yield strength, ultimate strength, and fracture elongation that are calibrated to match those reported above for the reduced model, and these values differ in some cases from those assumed by Sadek et al. (2008). Perhaps most significantly, Sadek et al. (2008) assumed a fracture elongation of 25 % for the wire reinforcement, while both the detailed and reduced models in this study assume a fracture elongation of 5 %.
- **Concrete modeling:** The most significant difference between the detailed model used in this study and that of Sadek et al. (2008) is in the modeling of concrete. The detailed model in this study uses both a different material model than Sadek et al. (2008) and different hourglass control parameters to suppress spurious modes of deformation in the reduced-integration solid elements. Parametric studies reported by Main and Sadek (2012, section 4.2.2) indicate that the combined effect of these differences results in an ultimate capacity for the detailed model in this study that is about 30 % larger than that obtained by Sadek et al. (2008). The detailed model in this study uses a continuous surface cap model for concrete (material type 159 in LS-DYNA), which incorporates a hardening cap that can expand and contract, smoothly intersecting the shear yield surface. This model can capture confinement effects and softening behavior in both tension and compression due to brittle and ductile damage accumulation. Detailed documentation of the material model is provided by Murray et al.

(2007). Default parameters recommended by Murray et al. (2007) are used in the model, based on a compressive strength of 20.7 MPa. An assumed strain co-rotational stiffness form of hourglass control was selected (hourglass control type 6 in LS-DYNA), and an hourglass control coefficient of $QM = 0.03$ was found sufficient to limit the energy associated with hourglass modes and achieve convergence in the computed results (Main and Sadek 2012, section 4.2.2).

Comparison of Detailed and Reduced Model Results

In comparing the detailed and reduced model results, two different methods of quasi-static loading are considered, as described in Alashker et al. (2010). The first method involves applying a concentrated load to the unsupported center column under displacement control, while the second method involves applying a gradually increasing uniform load to the entire slab under force control. Both types of analysis are performed using explicit time integration, in order to avoid convergence problems encountered by implicit methods and to enable the analyses to progress beyond local failures to evaluate the ultimate capacity of the system. While the solution method is dynamic in nature, quasi-static loading conditions are maintained by applying the loading as a gradually increasing function of time over a duration of several seconds. Both the applied load and the total vertical reaction at the column bases are computed in the analyses, and the load carried by the system is taken as the smaller of these values, in order to avoid overestimating the capacity of the system due to transient effects associated with local failures (see Main and Sadek 2012, section 4.1).

Fig. 9 shows a comparison of load-displacement curves obtained using the detailed and reduced models of the 2 bay \times 2 bay floor system under (a) concentrated loading and (b) uniform loading. Values of load intensity are plotted on the vertical axis for both concentrated and uniform loading, and the load intensity for concentrated loading is calculated by dividing the applied load by the tributary area of 55.7 m^2 for the center column. As noted by Alashker et al. (2009), the capacity of the system obtained using the two loading methods is comparable when presented in terms of load intensity. Since the

displacement of the center column is not meaningful after the connections have failed and the column has completely detached from the beams and girders, the vertical displacement plotted on the horizontal axes in Fig. 9 (and in subsequent figures) is the largest vertical displacement of the beam and girder ends originally attached to the center column. Prior to connection failure, this displacement matches very closely the displacement of the center column.

Good general agreement is observed between the detailed and reduced models in Fig. 9, providing verification of the reduced modeling approach. Under concentrated loading [Fig. 9(a)], both the detailed and reduced models show that all connections to the center column have completely failed at a displacement of about 650 mm, after which no further load can be applied to the system. Under uniform loading [Fig. 9(b)], the reduced model is quite consistent with the detailed model up to the initial peak load at a displacement of about 600 mm, prior to failure of the connections to the center column. After failure of these connections, the system continues to carry load as the floor slab bridges across the failed connections, and the detailed model predicts load values that are slightly greater than those from the reduced model. The slightly larger strength predicted by the detailed model is partly a consequence of the resistance of the steel deck to extension in the across-rib direction, which is neglected in the reduced model (see Fig. 4). However, the differences between the detailed and reduced model remain fairly small, and the predictions of the reduced model are conservative. Throughout the remainder of this paper, results are presented using the reduced modeling approach.

Analysis of Sudden Column Loss

While the previous section described procedures for quasi-static pushdown analysis with a missing column, the demands imposed under sudden column loss are higher than those under static loading. Gudmundsson and Izzuddin (2010) discuss the “sudden column loss” idealization and note that it provides a useful event-independent design scenario for disproportionate collapse assessment. The following subsections describe two approaches for analysis of sudden column loss.

Direct Dynamic Analysis

The procedure used for direct dynamic analysis of sudden column loss is similar to that presented by Alashker et al. (2010) and is illustrated in Fig. 10 using analysis results from the 2 bay \times 2 bay floor system (Fig. 3). Uniform gravity loading denoted w_1 is first applied gradually over a period of 1 s using a smooth ramp function and is held constant. At $t = 1.25$ s, the vertical support of the center column is suddenly removed. As shown in the inset of Fig. 10, the column drops vertically to a peak dynamic displacement denoted Δ_1 before rebounding and oscillating about a new equilibrium position. By repeating this analysis procedure for different levels of the uniform load intensity w_k , and calculating in each case the peak displacement Δ_k , discrete points on a load-displacement curve for sudden column loss can be generated, as illustrated in Fig. 10. Different values of the load intensity w_k are achieved in the computational model by adding distributed mass to the floor slab in addition to the self-weight. Gravity loading is applied by imposing body forces due to gravitational acceleration in the model. In this manner, both the gravity loading and the inertia of the structure are correctly represented. The resulting curve represents the relationship of the load intensity to the peak displacement after sudden column loss.

Energy-Based Approximate Analysis

While the procedure described in the previous section requires a separate dynamic analysis to be performed for each load-intensity, a load-displacement curve for sudden column loss can be generated more efficiently using an energy-based procedure similar to that previously used by Powell (2003), Guo and Gilsanz (2003), and Izzuddin et al. (2008). This procedure, which is summarized here in a somewhat different form for uniformly distributed loading, is based on the assumption that the structure responds in a single mode of deformation, whereby it can be analyzed as a single-degree-of-freedom system. In a sudden column loss scenario, the external work done by the applied loads in reaching the peak dynamic displacement Δ_o can be expressed as

$$W_{SCL}(\Delta_o) = \alpha w_{SCL} \Delta_o = U(\Delta_o) \quad (3)$$

where w_{SCL} is the uniform load that produces a peak displacement of Δ_o after sudden column loss, α is a constant that depends on the deformation mode, and $U(\Delta_o)$ is the internal energy in the system, which equals the external work because the kinetic energy is zero at the peak displacement. Assuming the same deformation mode under static loading, the external work at displacement Δ_o can be expressed as

$$W_{static}(\Delta_o) = \alpha \int_0^{\Delta_o} w_{static}(\Delta) d\Delta = U(\Delta_o) \quad (4)$$

where the function $w = w_{static}(\Delta)$, illustrated in Fig. 11, represents a load-displacement curve obtained from quasi-static pushdown analysis under uniform load. Because the same deformation mode is assumed, the internal energy $U(\Delta_o)$ is the same for static loading and sudden column loss. Equating Eqs. (3) and (4) then allows the constant α to be eliminated:

$$w_{SCL} \Delta_o = \int_0^{\Delta_o} w_{static}(\Delta) d\Delta \quad (5)$$

The right-hand side of Eq. (5) represents the shaded area in Fig. 11, while the left-hand side represents the hatched area. Eq. (5) then yields the following expression for the load intensity w_{SCL} that yields a peak dynamic displacement of Δ_o after sudden column loss:

$$w_{SCL} = \frac{1}{\Delta_o} \int_0^{\Delta_o} w_{static}(\Delta) d\Delta \quad (6)$$

By evaluating Eq. (6) with varying Δ_o , the function $w = w_{SCL}(\Delta)$ can be obtained, which represents the load-displacement curve for sudden column loss, shown by the dashed curve in Fig. 11. In this manner, the dynamic enhancement associated with sudden column loss can be included using only the results from a static pushdown analysis. The dynamic increase factor, denoted $\Omega(\Delta)$, can be defined as follows:

$$\Omega(\Delta) = \frac{w_{static}(\Delta)}{w_{SCL}(\Delta)} \quad (7)$$

Ultimate Capacity under Sudden Column Loss

While Izzuddin et al. (2008) used a limit state of first connection failure in assessing structural capacity, the quasi-static pushdown analysis procedure described previously, using explicit time integration with

uniform loading under force control, allows the quasi-static load-displacement curve $w = w_{static}(\Delta)$ to be evaluated beyond the initial failure of connections to assess the ultimate static capacity of a structural system. Let Δ_u denote the vertical column displacement corresponding to the ultimate static capacity, as illustrated in Fig. 11. It is evident in Fig. 11 that the function $w = w_{SCL}(\Delta)$ can continue to increase for displacements exceeding Δ_u , due to residual, post-ultimate resistance of the structural system. Provided that $w_{static}(\Delta) > w_{SCL}(\Delta)$, the analysis predicts that collapse will not occur. However, uncertainties in model predictions increase significantly in the post-ultimate response, particularly given the force-controlled nature of the uniform loading protocol, which produces accelerations and increasing dynamic effects after the ultimate capacity of the system is exceeded. The assumption of an unchanging mode of deformation, inherent in Eq. (6), may also become less appropriate after the ultimate load has been exceeded and displacements become very large. For these reasons, and for the sake of conservatism, the ultimate capacity under sudden column loss, denoted $w_{SCL,u}$, is evaluated at the displacement Δ_u corresponding to the ultimate static load (see Fig. 11):

$$w_{SCL,u} = w_{SCL}(\Delta_u) \quad (8)$$

A maximum permissible displacement Δ_{max} can also be introduced, so that if the uniform load $w_{static}(\Delta)$ is still increasing at Δ_{max} , the ultimate static load is limited to its value at this displacement:

$$w_{static}(\Delta_u) = \max_{0 < \Delta \leq \Delta_{max}} [w_{static}(\Delta)] \quad (9)$$

In this study, $\Delta_{max} = 1300$ mm is selected, which corresponds to the approximate displacement at which erosion of shell elements, representing fracture of the steel deck, is first observed for the 2 bay \times 2 bay floor system in Fig. 3. In almost all cases, the ultimate static load occurs prior to Δ_{max} .

Analysis of Prototype Floor Systems

Comparison of Direct and Approximate Analysis Results

Fig. 12 shows load-displacement results for (a) 2 bay \times 2 bay and (b) 4 bay \times 4 bay floor systems from building A under loss of the center column. Fairly good agreement is observed between the results for sudden column loss using direct dynamic analysis (open circles) and energy-based approximate analysis (dashed curves), with differences in the load intensity being generally less than 10 %. While initial connection failures (i.e., erosion of bolt springs) are observed for center column displacements of about 400 mm, Fig. 12 shows good agreement between the direct and approximate analysis results for much larger displacements, confirming that the approximate procedure illustrated in Fig. 11 remains applicable even after connection failures have occurred. Subsequent results in this paper use only the approximate procedure for analysis of sudden column loss.

Shown as horizontal lines in Fig. 12 are the two levels of gravity loading discussed previously: the load combination $1.2D + 0.5L_{office}$ from Eq. (1) and the lower level of expected gravity loading from Eq. (2). Fig. 12(a) shows that the ultimate capacity of the 2 bay \times 2 bay floor system under sudden column loss, $w_{SCL,u}$ from Eq. (9), is slightly less than the expected gravity loading. For the 4 bay \times 4 bay floor system, Fig. 12(b) shows that $w_{SCL,u}$ exceeds both the expected gravity loading and the larger level of gravity loading, with $w_{SCL,u}$ in this case corresponding to the maximum permissible displacement of $\Delta_{max} = 1300$ mm. The continuity provided by the adjoining bays in the 4 bay \times 4 bay floor system is found to increase its capacity under sudden column loss by 63 % relative to the 2 bay \times 2 bay floor system. Because real buildings generally comprise more than two bays in each direction, their floor systems can usually benefit from such continuity. The influence of slab continuity is further discussed subsequently.

Influence of Post-Ultimate Connection Behavior

Fig. 13 shows plots comparable to those in Fig. 12, but based on an assumption of sudden fracture, rather than gradual softening, in the post-ultimate behavior of the connections (see Fig. 7). Comparing Figs. 12

and 13 shows that sudden connection fracture reduces $w_{SCL,u}$ by 17 % for the 2 bay \times 2 bay system and by 13 % for the 4 bay \times 4 bay system. While these reductions are significant, it is noted that reductions by as much as 23 % in peak vertical capacity were observed for two-span beam assemblies without floor slab for sudden fracture vs. gradual softening (Main and Sadek 2012, section 3.5.3). The contribution of the floor slab is thus found to make the composite framing systems somewhat less sensitive to the effect of sudden connection failure than the bare steel framing system. For the sake of conservatism, all subsequent analyses in this report use connection models that represent sudden fracture in the post-ultimate response.

Influence of Slab Continuity

Fig. 13 shows that the ultimate capacity $w_{SCL,u}$ of the 4 bay \times 4 bay floor system is 71 % larger than that of the 2 bay \times 2 bay system. Insight into this enhanced capacity is afforded by considering the corresponding forces in the beams and the floor slab, as shown in Fig. 14(a) for the 2 bay \times 2 bay floor system and in Fig. 14(b) for the 4 bay \times 4 bay floor system. Forces are shown along the edges of the bay immediately to the northwest of the missing center column, and alphanumeric column designations at each corner of the isolated bay correspond to the grid systems shown in Fig. 1(a) and in Fig. 3 for the 4 bay \times 4 bay and 2 bay \times 2 bay floor systems, respectively. Axial forces at the beam ends are shown using arrows, and numerical values of axial force are indicated, with positive values denoting tension. Tensile forces normal to the slab edges are shown using filled areas along the slab edges, and peak values of force per length are indicated. The forces in Fig. 14 were obtained under quasi-static loading. However, analysis results indicated that internal forces at the same level of displacement under sudden column loss are comparable to those under quasi-static loading (discrepancies are generally less than 15 %, with some larger local discrepancies in the slab edge forces). Since internal forces depend directly on the structural deformations, this is consistent with the assumption in the energy-based approximate analysis presented above, that the deformation mode under static loading is the same as under sudden column loss. Dynamic effects influence the response of the system not primarily through differences in internal forces at a given

displacement, but through the fact that the internal forces are partially balanced by inertial forces, thus reducing the uniform load that can be sustained.

The values of tensile force per unit length in Fig. 14 do not include concrete forces, because the focus here is on components with sufficient ductility to potentially serve as horizontal ties in the floor system and on determining the tensile forces that these components must sustain. Although concrete provides some initial tensile resistance prior to cracking, this resistance is depleted for tensile strains exceeding 0.25 % in the reduced model, as noted previously. Therefore, forces normal to the ribs in the steel deck (west and east edges in Fig. 14) correspond only to the tension in the welded wire reinforcement, while forces along the ribs (north and south edges in Fig. 14) include tension from both the wire reinforcement and the steel deck. In some cases, flexure of the slab caused the steel deck to be in compression while the wire reinforcement was in tension, or vice versa. The compressive component was not included in such cases to prevent cancellation of forces that would obscure the true magnitude of tension sustained by one component or the other. Tensile forces along interior edges of the bay were calculated as the larger tensile value from the elements on either side of the edge. Note that because only tensile forces in the steel components are included in Fig. 14, these do not represent the net forces in equilibrium with the surrounding structure.

Fig. 14(a) shows forces in the 2 bay \times 2 bay system at the ultimate static load, while Fig. 14(b) shows forces in the 4 bay \times 4 bay system at a comparable displacement of the center column. Comparable forces are observed along the south and east edges of the isolated bays, but tensile forces along the north and west edges are significantly larger for the 4 bay \times 4 bay system than for the 2 bay \times 2 bay system, due to continuity of the floor slab. The larger tensile forces in the slab along the north and west edges are associated with much larger values of axial compression at the beam ends, indicating the development of a negative bending moment through composite action of the beams and slab. Such flexural resistance, which is developed at the beam ends opposite the missing column, is much more pronounced in Fig. 14(b) than in Fig. 14(a) and contributes to the enhanced capacity of the 4 bay \times 4 bay system.

Near-Penultimate Column Loss

Fig. 15(a) shows load-displacement curves for the 4 bay \times 4 bay floor system under loss of near-penultimate column D4 [see Fig. 1(a)], for which the ultimate capacity $w_{SCL,u}$ is about 19 % less than that under loss of the center column [Fig. 13(b)], due to the lack of slab continuity along two edges of the affected bays. The ultimate capacity $w_{SCL,u}$ in Fig. 15(a) is adequate to sustain the expected gravity loading but not the higher level of gravity loading. Fig. 15(b) shows comparable load-displacement curves for loss of near-penultimate column D3 in the 3 bay \times 4 bay gravity framing system from building B [see Fig. 1(b)]. Fig. 15(b) shows that the ultimate capacity $w_{SCL,u}$ of the 3 bay \times 4 bay system from building B is inadequate to sustain even the expected gravity loading. Noting that building B has longer spans in the N-S direction than building B, Fig. 15 shows that the floor system with longer spans (and correspondingly larger tributary areas) is more susceptible to collapse than the floor system with shorter spans.

Assessment of Current Tie Force Requirements

2009 International Building Code

The structural integrity requirements in the 2009 IBC (ICC 2009, Section 1614) include the following requirement for the end connections of beams and girders in steel frame structures:

$$T_n \geq \frac{2}{3} V_u \quad (10)$$

where T_n is the nominal tensile strength and V_u is the required shear strength, using the notation of AISC 360-10 (AISC 2010) for LRFD. Geschwindner and Gustafson (2010) previously showed that all properly designed single-plate shear connections comply with this requirement. For shear connections in the prototype floor systems, the ratio T_n/V_u ranges from 2.01 to 2.20 (Main and Sadek 2012, section 5.4.1), indicating that the nominal tensile strength is more than three times greater than required.

Although the shear tab connections considered in this study satisfy the structural integrity requirements of the 2009 IBC, it was observed in Fig. 15(b) that the 3 bay \times 4 bay floor system from

building B is unable to sustain sudden column loss under the expected gravity loading. It can therefore be concluded that the structural integrity requirements of the 2009 IBC are not always sufficient to prevent collapse under sudden column loss. In addition, for cases in which collapse of the floor system is arrested, the connections are called upon to carry axial forces that substantially exceed the tensile strength required by the 2009 IBC. Consider the 4 bay \times 4 bay floor system from building A, which can sustain sudden loss of the center column under the expected gravity loading with a peak dynamic displacement of about 320 mm [Fig. 13(b)]. The connections in the North-South direction for this floor system fail at a displacement of about 210 mm, sustaining a peak tensile force of 314 kN prior to failure, which is 3.1 times larger than the tensile strength required by the 2009 IBC.

Unified Facilities Criteria 4-023-03

Because the shear connections considered in this study are unable to sustain tensile forces while undergoing rotations of 0.20 rad (see Main and Sadek, section 5.3.3), the UFC 4-023-03 (DOD 2009, Section 3-1) requires the horizontal tie forces to be carried by the floor system. The required strength of transverse and longitudinal ties (DOD 2009, Section 3-1.3.1.1) is given by

$$F_i = 3w_F L_1 \quad (11)$$

where $w_F = 1.2D + 0.5L$ is the uniform floor load, consistent with the load combination in Eq. (1), and L_1 is the distance between the centers of the columns in the direction under consideration. The required strength of peripheral ties (DOD 2009, Section 3-1.3.2) is given by

$$F_p = 6w_F L_1 L_p \quad (12)$$

where $L_p = 0.91$ m (DOD 2009, Section 3-1.3.2). Values of the required tie forces were calculated by setting w_F in Eqs. (11) and (12) equal to the combined floor load of $1.2D + 0.5L_{office}$ from Eq. (1).

To develop the required tie forces in the prototype floor systems, reinforcing bars were incorporated in the floor slabs in addition to the welded wire reinforcement. The added reinforcing bars were designed to carry all of the required tie forces, and no contribution from the steel deck and welded

wire reinforcement was considered. The reinforcing bars are represented in the computational model using beam elements that share common nodes with the shell elements representing the floor slab, assuming that the reinforcement remains fully bonded to the surrounding concrete. The reinforcing steel is represented using a piecewise-linear plasticity model, with the yield strength, tensile strength, and elongation at fracture based on the minimum specified values for ASTM A615 Grade 60 steel. Details on the size, placement, and modeling of added reinforcement are provided by Main and Sadek (2012).

Fig. 16 shows plots corresponding to those in Fig. 15, but for floor systems that incorporate additional reinforcement to satisfy the horizontal tie force requirements of UFC 4-023-03. Comparing Figs. 15 and 16 shows that the horizontal ties approximately double the capacity of the floor systems under static loading and increase their capacity under sudden column loss by about 50 %. In contrast with Fig. 15, the ultimate capacity $w_{SCL,u}$ exceeds the gravity loading of $1.2D + 0.5L_{office}$ for both floor systems in Fig. 16, demonstrating the effectiveness of the horizontal ties specified by UFC 4-023-03.

Evaluation of Required Tie Forces

To investigate the tie forces that must be developed in the floor slab to sustain specified levels of gravity loading, enhanced floor slabs with increased deck thickness and reinforcement area are considered, as listed in Table 1. Floor slab S16-2.5 is considered for prototype building A, while floor slabs S16-5 and S16-14 are considered for building B. The enhanced slabs incorporate a 16 gage steel deck, which is the maximum standard deck thickness (ANSI/SDI 2006). Standard wire sizes (ASTM 2007) are considered for the welded wire reinforcement, and the grid spacing is 152 mm \times 152 mm in all cases.

Fig. 17 summarizes the influence of floor slab reinforcement on the capacity of (a) the 4 bay \times 4 bay floor system from building A and (b) the 3 bay \times 4 bay floor system from building B under sudden loss of near-penultimate columns. All curves were obtained using the energy-based approximate analysis of sudden column loss, and solid circles on each curve indicate the ultimate capacity under sudden column loss, $w_{SCL,u}$ from Eq. (8). Fig. 17(a) shows that the enhanced slab S16-2.5 enables the floor system

to sustain the gravity loading of $1.2D + 0.5L_{office}$ without collapse. Fig. 17(b) shows that the enhanced slab S16-5 enables the floor system to sustain the expected gravity loading, while the enhanced slab S16-14 enables the floor system to sustain the higher gravity loading of $1.2D + 0.5L_{office}$.

Gray vertical lines in Figs. 17(a) and 17(b) indicate the center column displacements at which initial connection failures occur, and in both cases, the curves corresponding to different levels of reinforcement differ only slightly prior to the initial connection failure. This indicates that connection failures occur before the tie forces can contribute significantly to the structural resistance. Fig. 17 shows that even with the highest level of reinforcement, the floor system is unable to sustain the expected gravity loading prior to connection failure. For large displacements of the center column, after connection failures have occurred and membrane action in the slab has developed, the tie forces in the slab are found to significantly increase the ultimate capacity of the floor system. This confirms the appropriateness of the requirement in UFC 3-023-03 (DOD 2009, section 3-1) that tie forces should be carried by the floor slab rather than by the beams, unless the beam-to-column connections can be shown to sustain the required tie forces while undergoing significant rotations.

Fig. 18 shows edge forces at the ultimate static load from the three analysis cases presented in Fig. 17(a). These plots were generated using the same procedure described previously for Fig. 14, isolating the bay immediately to the northwest of the missing column. Fig. 18 clearly shows increases in the tensile forces along the slab edges with increasing levels of slab reinforcement. In all cases, the connections to the missing column failed prior to reaching the ultimate load, as indicated by zero forces at the beam ends. Composite action is also evident in all cases, with substantial compressive forces at the beam ends along the north and west edges being accompanied by tensile forces in the floor slab, together providing negative flexural resistance along these edges. In some cases, compressive axial forces that exceed the capacity of the connection are observed; these cases are associated with binding of the beam flange against the column, as represented in the model by the “gap spring” shown in Fig. 5.

The slab edge forces in Fig. 18 can be used to assess the tie forces necessary to sustain different levels of gravity loading without collapse. In making this assessment, it is useful to compare with the required strength of the transverse and longitudinal ties from UFC 4-023-03 (DOD 2009), which are given in Eq. (11) and can be written in the following alternative form:

$$F_i / L_1 = 3w_F \quad (13)$$

The quantity F_i / L_1 , obtained by dividing the tie force per length by the span length, has units of force per area and is denoted the “normalized tie force.” Peak values of the normalized tie force for each case in Fig. 18 are obtained by identifying the peak value of F_i (the tie force per length) in each span direction and then dividing these values by the corresponding span length L_1 . The larger of the two values of F_i / L_1 in either span direction is the governing value of the normalized tie force sustained by the floor system.

Fig. 19(a) shows a plot of the governing values of the normalized tie forces from Fig. 18 against the ultimate capacities of the floor systems under quasi-static loading. Also included in Fig. 19(a) are corresponding results for the 3 bay \times 4 bay floor system from building B from three of the four analysis cases in Fig. 17(b), for which slab edge forces are presented in Main and Sadek (2012, section 5.5). The values plotted in Fig. 19(a) indicate the relationship between the tie forces carried by the system and the uniform static load that can be sustained. The computed values for buildings A and B collapse fairly well along a single curve that can be approximated by the following relationship, shown in Fig. 19(a):

$$F_i / L_1 = \frac{w_F^2}{(3.125 \text{ kN/m}^2)} \quad (w_F \text{ and } F_i / L_1 \text{ in kN/m}^2) \quad (14)$$

Eq. (13) from UFC 4-023-03 (DOD 2009) is also shown in Fig. 19(a) for comparison, as the intent of both relationships is to indicate the tie forces required to sustain a particular level of loading. The two expressions intersect at a load intensity of $w_F = 9.38 \text{ kN/m}^2$, which is about 1.73 times larger than the combined gravity loading of $1.2D + 0.5L_{office}$. For loads less than this value, the computed tie forces are less than required by Eq. (13), indicating that the UFC is conservative. For loads greater than this value, the computed tie forces exceed those required by Eq. (13), indicating that the UFC is not conservative.

While the results in Fig. 19(a) are for quasi-static loading, Fig. 19(b) presents a corresponding plot for sudden column loss, in which the governing values of F_i / L_1 are plotted against values of $w_{SCL,u}$. The computed values no longer collapse along a single curve due to variability in the dynamic increase factor Ω defined in Eq. (7). Eq. (14) can be modified as follows to incorporate Ω :

$$F_i / L_1 = \frac{(\Omega w_F)^2}{(3.125 \text{ kN/m}^2)} \quad (w_F \text{ and } F_i / L_1 \text{ in kN/m}^2) \quad (15)$$

Eq. (15) is plotted in Fig. 19(b) for both $\Omega = 1.68$ and $\Omega = 1.16$, which represent the largest and smallest values of $\Omega(\Delta_u) = w_{static}(\Delta_u) / w_{SCL,u}$ obtained from the different floor systems, and the two curves capture fairly well the upper and lower limits of the computed values. A general trend of increasing $\Omega(\Delta_u)$ with increasing slab reinforcement is evident in the results, with more lightly reinforced slabs falling near the curve for $\Omega = 1.16$, and more heavily reinforced slabs falling near the curve for $\Omega = 1.68$. Smaller values of Ω for lightly reinforced floor slabs are a consequence of the fact that these systems exhibit a clear plateau in the load-displacement curve (e.g., Fig. 15), where for an elastic-plastic response, Ω decreases to approach unity at large displacements. Larger values of Ω for more heavily reinforced slabs are a consequence of the stiffer, more linear response that these systems exhibit up to the ultimate load (e.g., Fig. 16), where a linear response corresponds to a value of $\Omega = 2$.

Eq. (13) from UFC 4-023-03 (DOD 2009) is also shown in Fig. 19(b), and the intersection points occur at load intensities of $w_F = 3.32 \text{ kN/m}^2$ for $\Omega = 1.68$ and $w_F = 6.97 \text{ kN/m}^2$ for $\Omega = 1.16$. For a particular value of Ω , Eq. (13) is conservative for loads below the intersection point and is not conservative for loads above this point. Eq. (15) is proposed as a replacement for Eq. (13) from UFC 4-023-03 for steel frame systems with composite floor systems, as it more accurately captures the nonlinear behavior observed in the computations and allows dynamic effects associated with sudden column loss to be incorporated directly through the parameter Ω . The upper-bound value of $\Omega = 1.68$, applicable to the heavily reinforced floor slabs in this study, could be conservatively used in design. Additional analyses

using the energy-based procedure of Fig. 11 may also enable the development of guidelines for selecting an appropriate value of Ω as a function of the slab reinforcement.

Conclusions

This paper presented a computational assessment of the performance of steel gravity framing systems with single-plate shear connections and composite floor slabs under column loss scenarios. The computational assessment used a reduced modeling approach, while comparisons with detailed model results were presented to establish confidence in the approach. Both quasi-static loading and sudden column loss were considered, and an energy-based approximate procedure for analysis of sudden column loss was adopted, after verification through comparisons with direct dynamic analyses, further enhancing the efficiency of the reduced modeling approach. Reduced models were used to investigate the influence of factors such span length, slab continuity, and the mode of connection failure on the collapse resistance of gravity frame systems, and the following main conclusions were reached:

1. Sudden fracture of shear connections after reaching the ultimate load reduces the ultimate capacity of gravity frame systems under sudden column loss scenarios by as much as 17 % compared to a gradual softening behavior associated with bolt tear-out. It is recommended that sudden fracture should be conservatively assumed in modeling and analysis of shear connections.
2. The effect of slab continuity beyond the bays adjoining the missing column was found to be significant, with the ultimate capacity of a 4 bay \times 4 bay floor system under sudden loss of the center column being 71 % larger than that of a corresponding 2 bay \times 2 bay system.
3. Longer span lengths, with correspondingly larger tributary areas, were found to result in reduced capacities under column loss scenarios, with the ultimate capacity under sudden loss of a near-penultimate column being 18 % lower for prototype building B than for prototype building A.
4. The structural integrity requirements in the 2009 IBC (ICC 2009) were found to be insufficient for preventing collapse under column loss scenarios.

5. The tie force requirements in UFC 4-023-03 were found to be conservative for quasi-static uniform load intensities less than 9.38 kN/m^2 , while for quasi-static loads exceeding this value, computed tie forces exceeded those required by the UFC.
6. An empirical equation was developed that relates the required tie force levels to the uniform load on the slab, capturing well the observed nonlinearity in the computed structural responses and accounting for dynamic enhancement due to sudden column loss.

While this study addressed the tie forces necessary to prevent collapse under column loss scenarios, the analyses conducted in this study assumed continuity of the steel deck and welded wire reinforcement. Detailing requirements to ensure adequate continuity of load paths through the composite floor system need to be considered to enable the required tie forces to be developed.

Acknowledgments

Valuable comments and input on this work were provided by Fahim Sadek, H.S. Lew, and Yihai Bao of NIST, Judy Liu of Purdue University, and Sam-Young Noh of Hanyang University. Helpful exchanges with Bruce Ellingwood (Georgia Tech) and David J. Stevens (Protection Engineering Consultants) during the course of this work are also gratefully acknowledged.

Disclaimer

Certain commercial entities, equipment, products, or materials are identified in this document in order to describe a procedure or concept adequately. Such identification is not intended to imply recommendation, endorsement, or implication that the entities, products, materials, or equipment are necessarily the best available for the purpose.

References

- Alashker, Y. and El-Tawil, S. (2011). "A design-oriented model for the collapse resistance of composite floors subjected to column loss." *Journal of Constructional Steel Research*, 67, 84-92.
- Alashker, Y., El-Tawil, S. and Sadek, F. (2010). "Progressive Collapse Resistance of Steel-Concrete Composite Floors." *Journal of Structural Engineering*, 136(10), 1187-1196.
- Alashker, Y., Li, H. and El-Tawil, S. (2011). "Approximations in progressive collapse modeling." *Journal of Structural Engineering*, 137(9), 914-924.
- American Society of Civil Engineers (ASCE). (2010). "Minimum design loads for buildings and other structures." *ASCE/SEI 7-10*, Reston, VA.
- American Institute of Steel Construction (AISC). (2010). "Specification for structural steel buildings." *ANSI/AISC 360-10*, Chicago, IL.
- American National Standards Institute (ANSI). (1982). "Minimum design loads for buildings and other structures." *ANSI A58*, New York.
- American National Standards Institute/Steel Deck Institute (ANSI/SDI). (2006). "Standard for composite steel floor deck." *C1.0 – 2006*. <<http://www.sdi.org/ansi/C1SDIANSI.pdf>> (accessed April 20, 2012)
- ASTM International. (2007). "Standard specification for steel wire, plain, for concrete reinforcement." *ASTM A82/A82M – 07*, West Conshohocken, PA.
- American Welding Society (AWS). (2010). "Structural welding code – steel." *AWS D1.1/D1.1M:2010*, Miami, FL.
- Cashell, K.A., Elghazouli, A.Y., and Izzuddin, B.A. (2011a). "Failure assessment of lightly reinforced floor slabs: I: Experimental investigation." *Journal of Structural Engineering*, 137(9), 977-988.
- Cashell, K.A., Elghazouli, A.Y., and Izzuddin, B.A. (2011b). "Failure assessment of lightly reinforced floor slabs: II: Analytical studies." *Journal of Structural Engineering*, 137(9), 989-1001.
- DOD (2009). *Design of Buildings to Resist Progressive Collapse*, Unified Facilities Criteria (UFC) 4-023-03, Department of Defense, 25 January 2009.

- Ellingwood, B.R., Smilowitz, R., Dusenberry, D.O., Duthinh, D., Lew, H.S., and Carino, N.J. (2007). “Best practices for reducing the potential for progressive collapse in buildings.” *NISTIR 7396*, National Institute of Standards and Technology, Gaithersburg, MD.
- Federal Emergency Management Agency (FEMA). (2000). “State of the art report on connection performance.” *FEMA 355D*, SAC Joint Venture and FEMA, Washington, D.C.
- Foley, C.M., Barnes, K., and Schneeman, C. (2008). “Quantifying and enhancing robustness in steel structures: Part 2 – Floor framing systems.” *Engineering Journal*, AISC, Fourth Quarter, 267-286.
- Geschwindner, L.F. and Gustafson, K.D. (2010). “Single-plate shear connection design to meet structural integrity requirements.” *Engineering Journal*, AISC, Third Quarter, 189-202.
- Gilbert, R.I. and Sakka, Z.I. (2007). “Effect of reinforcement type on the ductility of suspended reinforced concrete slabs.” *Journal of Structural Engineering*, 133(6), 834-843.
- Gudmundsson, G.V. and Izzuddin, B.A. (2010). “The ‘sudden column loss’ idealisation for disproportionate collapse assessment.” *The Structural Engineer*, 88(6), 22-26.
- Guo, W. and Gilsanz, R. (2003). “Simple nonlinear static procedure for progressive collapse evaluation.” Proceedings, Steel Building Symposium: Blast and Progressive Collapse Resistance, December 4-5, 2003, New York, 97-106,
- Hallquist, J. (2007). “LS-DYNA Keyword User’s Manual.” Livermore Software Technology Corporation, Livermore, CA.
- International Code Council (ICC). (2003). *International Building Code*, Falls Church, VA.
- Izzuddin, B.A., Vlassis, A.G., Elghazouli, A.Y., and Nethercot, D.A. (2008). “Progressive collapse of multi-storey buildings due to sudden column loss – Part I: Simplified assessment framework.” *Engineering Structures*, 30, 1308-1318.
- Kwasniewski, L. (2010). “Nonlinear dynamic simulations of progressive collapse for a multistory building.” *Engineering Structures*, 32, 1223-1235.

- Lew, H.S., Bao, Y., Sadek, F., Main, J.A., Pujol, S., and Sozen, M.A. (2011). "An experimental and computational study of reinforced concrete assemblies under a column removal scenario." *NIST Technical Note 1720*, National Institute of Standards and Technology, Gaithersburg, MD.
- Lew, H. S., Main, J. A., Robert, S. D., Sadek, F., and Chiarito, V. P., (2012). "Performance of steel moment connections under a column removal scenario. I: Experiments." *Journal of Structural Engineering*, 139(1), 98-107.
- Main, J.A., Bao, Y., Sadek, F., Lew, H.S. (2010). "Experimental and computational assessment of robustness of steel and reinforced concrete framed buildings." *Applications of Statistics and Probability in Civil Engineering: Proceedings of the 11th International Conference*, Held in Zürich, Switzerland, August 1-4, 2011, Taylor & Francis Group, London, 2184-2192.
- Main, J.A. and Sadek, F. (2012). "Robustness of steel gravity frame systems with single-plate shear connections." *NIST Technical Note 1749*, National Institute of Standards and Technology, Gaithersburg, MD.
- Main, J.A. and Sadek, F. (2013). "Modeling and analysis of single-plate shear connections under column loss." *Journal of Structural Engineering*, in press.
- Murray, Y.D., Abu-Odeh, A., and Bligh, R. (2007). "Evaluation of LS-DYNA concrete material model 159." *FHWA-HRT-05-063*, Federal Highway Administration, McLean, VA.
- Ollgaard, J.G., Slutter, R.G., and Fisher, J.W. (1971). "Shear strength of stud connectors in lightweight and normal weight concrete." *Engineering Journal*, AISC, 8(2), 55-64.
- Powell, G. (2003). "Collapse analysis made easy (more or less)." *Proceedings, 2003 Annual Meeting of the Los Angeles Tall Buildings Structural Design Council*, May 2003, Los Angeles, 1-14.
- Rambo-Roddenberry, M. (2002). "Behavior and strength of welded stud shear connectors." Ph.D. Dissertation, Virginia Polytechnic Institute and State University, Blacksburg, VA.

- Sadek, F., El-Tawil, S., and Lew, H.S. (2008). “Robustness of composite floor systems with shear connections: modeling, simulation, and evaluation.” *Journal of Structural Engineering*, 134(11), 1717-1725.
- Sadek, F., Main, J. A., Lew, H. S., and El-Tawil, S. (2012). “Performance of steel moment connections under a column removal scenario. II: Analysis.” *Journal of Structural Engineering*, 139(1), 108-119.
- Stevens, D. (2008). “Assessment and proposed approach for tie forces in framed and load-bearing wall structures.” *Final Report, Prepared for Security Engineering Working Group*, Protection Engineering Consultants, Dripping Springs, TX.
- Thompson, S.L. (2009) “Axial, shear and moment interaction of single plate ‘shear tab’ connections.” Master’s Thesis, Milwaukee School of Engineering, Milwaukee, WI.
- Weigand, J.M., Meissner, J.E., Francisco, T., Berman, J.W., Fahnestock, L.A., and Liu, J. (2012). “Overview of AISC/NSF structural integrity research and preliminary results.” *Proceedings, 2012 Structures Congress*, American Society of Civil Engineers, Reston, VA.

Table

Table 1. Properties of steel deck and welded wire reinforcement for floor slabs

Slab Designation*	Steel Deck Thickness	Wire size
S20-1.4 (original)	20 gage: $t = 0.91$ mm	W1.4: $A_w = 9.03$ mm ²
S16-2.5	16 gage: $t = 1.52$ mm	W2.5: $A_w = 16.1$ mm ²
S16-5	16 gage: $t = 1.52$ mm	W5: $A_w = 32.3$ mm ²
S16-14	16 gage: $t = 1.52$ mm	W14: $A_w = 90.3$ mm ²

* This is not a standard designation; it is simply used for convenience in this paper.

Figures

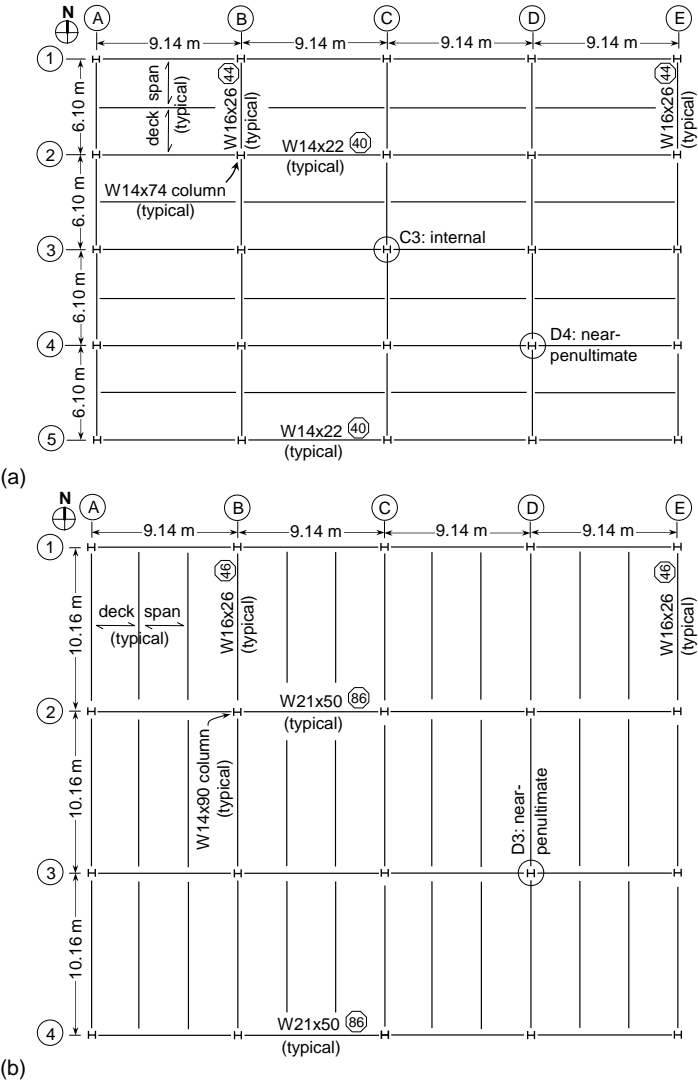


Fig. 1. Plan layouts for prototype composite floor systems: (a) 4 bay × 4 bay system from building A; (b) 3 bay × 4 bay system from building B (number of shear studs indicated next to beam and girder designations)

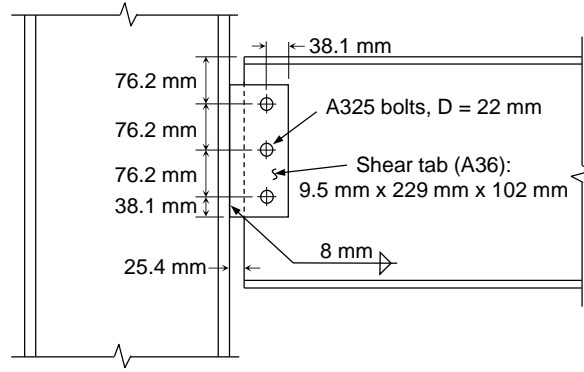


Fig. 2. Details of single-plate shear connection with three bolt rows

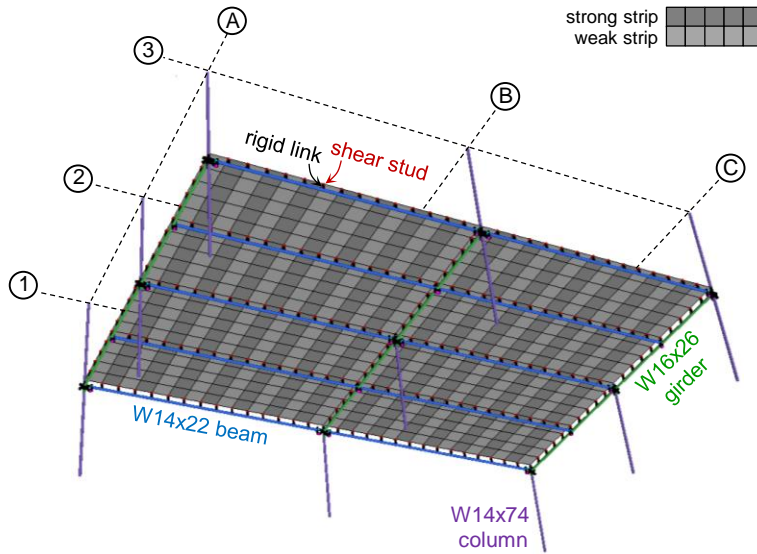


Fig. 3. Reduced model of 2 bay \times 2 bay composite floor system

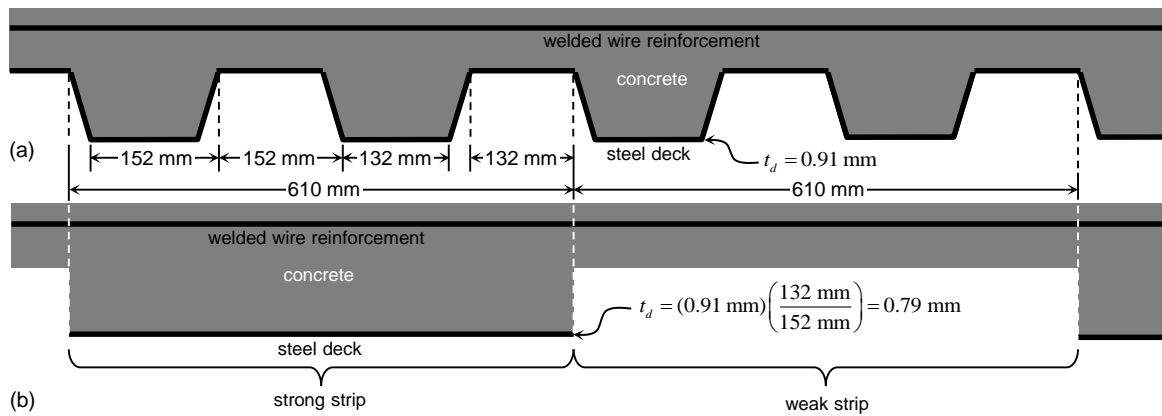


Fig. 4. Reduced modeling of composite floor slab: (a) actual profile; (b) alternating strong and weak strips

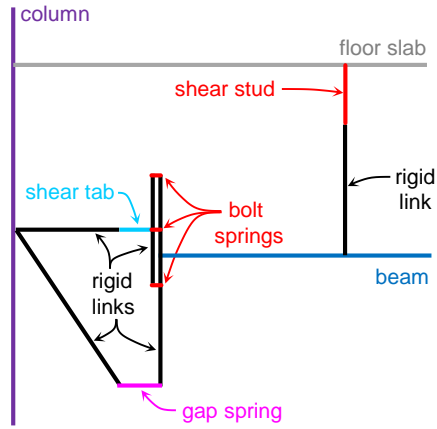


Fig. 5. Reduced modeling of shear studs and beam-to-column connections

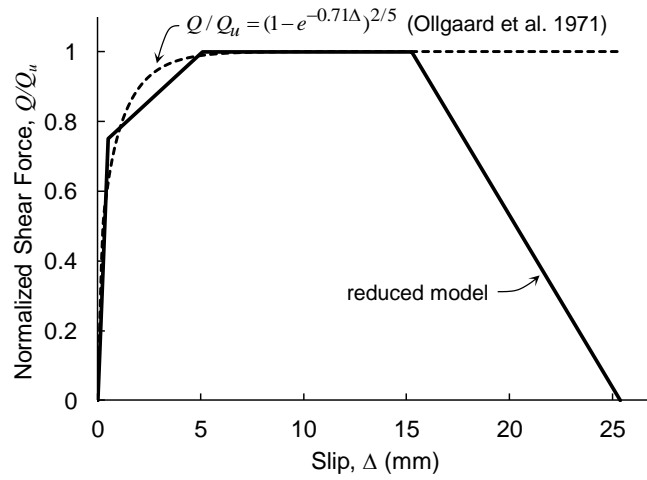


Fig. 6. Shear force versus slip relationship for shear studs used in reduced models

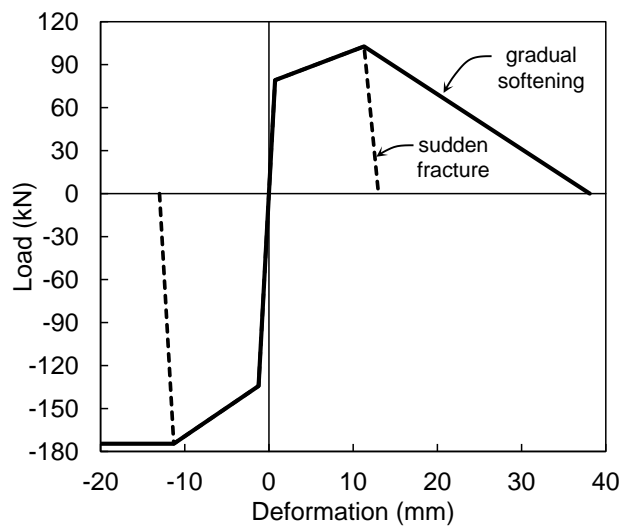


Fig. 7. Axial load-deformation relationships for bolt springs with alternate forms of post-ultimate behavior

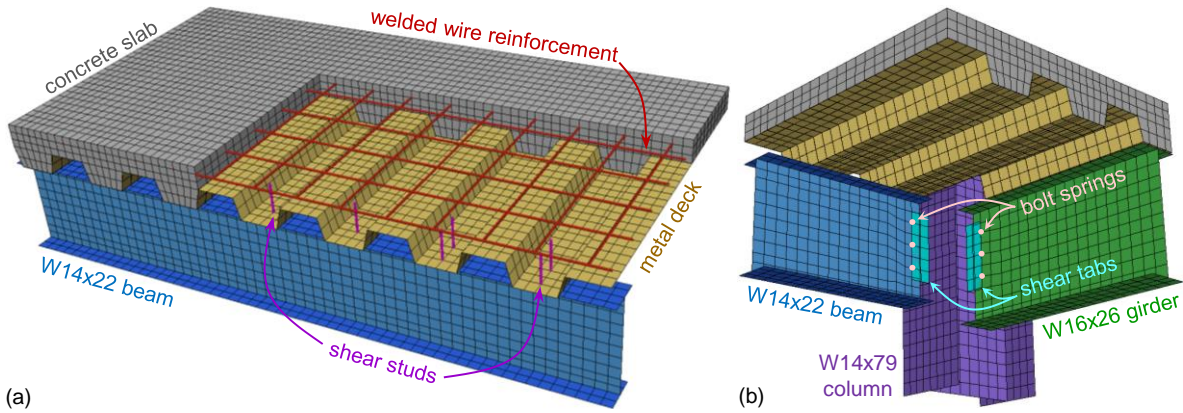


Fig. 8. Finite element mesh used in detailed model: (a) composite floor slab; (b) beam-to-column connections

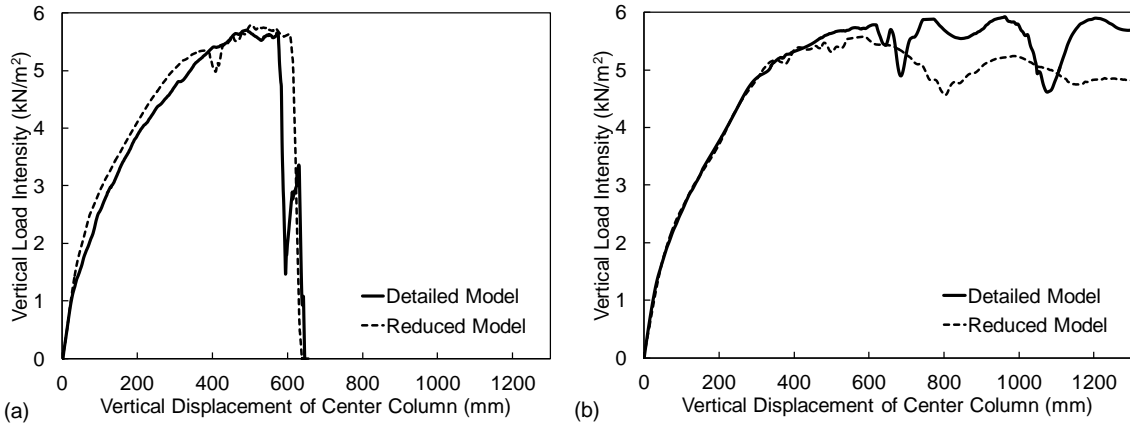


Fig. 9 Comparison of load-displacement curves from detailed and reduced models: (a) concentrated load; (b)

uniform load (2 bay \times 2 bay floor system from building A)

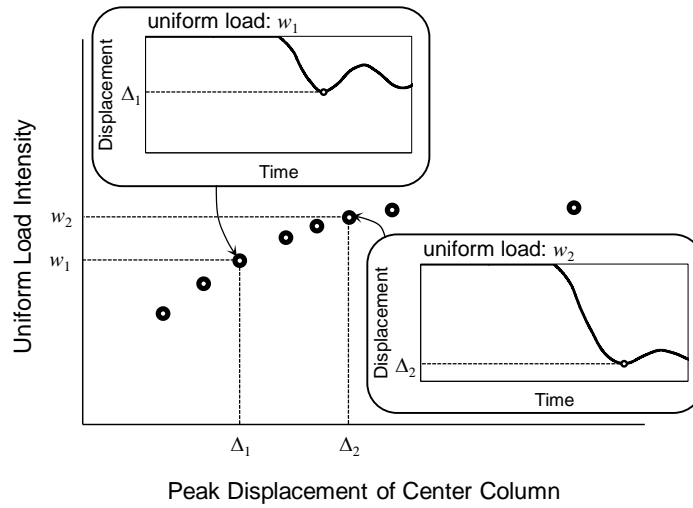


Fig. 10. Direct analysis procedure for generating a load-displacement curve for sudden column loss

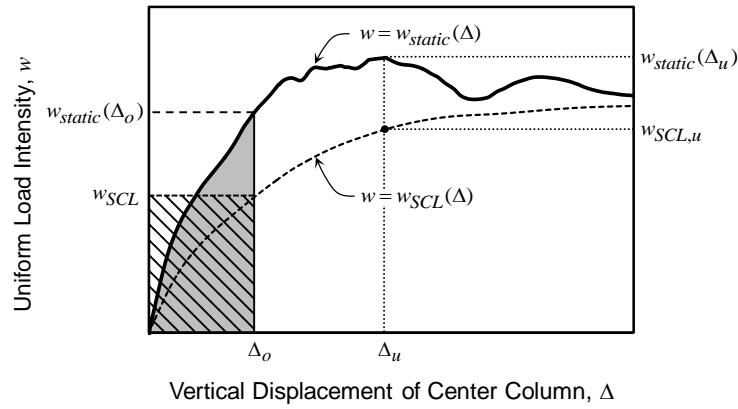


Fig. 11. Approximate procedure for generating a load-displacement curve for sudden column loss

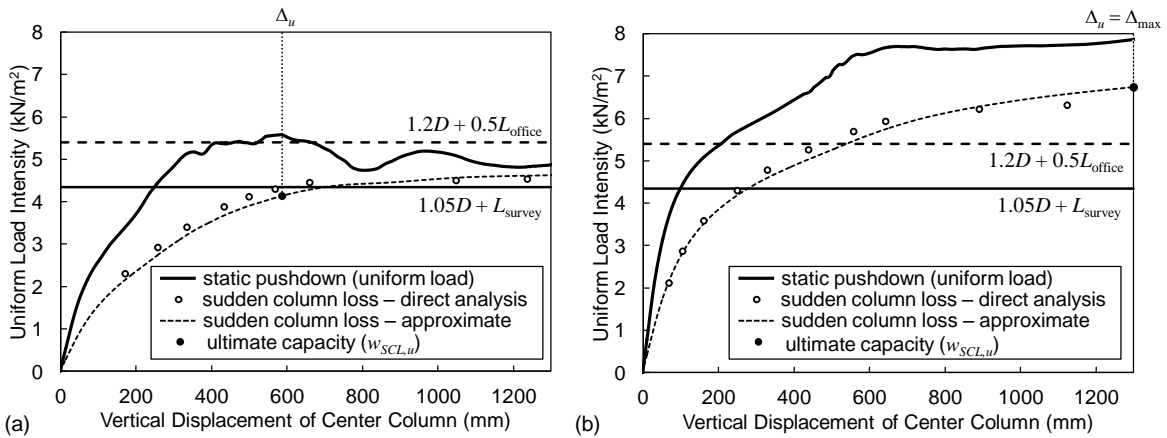


Fig. 12. Load-displacement curves under central column loss for floor systems from building A with gradual softening in post-ultimate response of connections: (a) 2 bay × 2 bay; (b) 4 bay × 4 bay

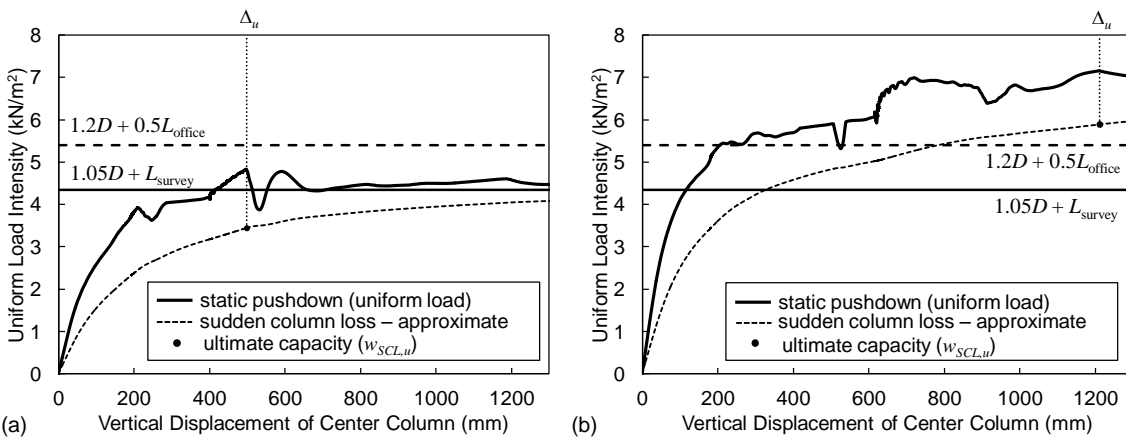


Fig. 13. Load-displacement curves under central column loss for floor systems from building A with sudden fracture in post-ultimate response of connections: (a) 2 bay \times 2 bay; (b) 4 bay \times 4 bay

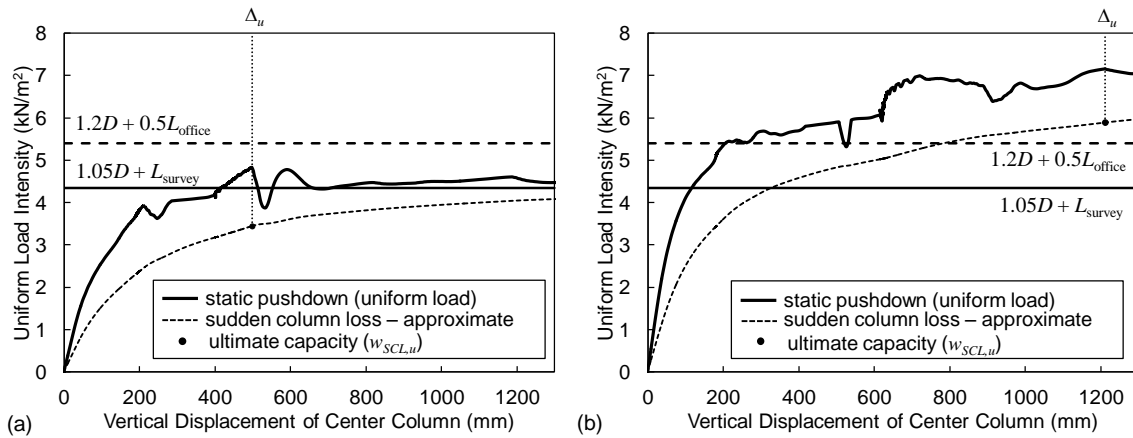


Fig. 14. Axial forces at beam ends (arrows) and tensile force per length normal to slab edges (filled areas) for (a) 2 bay \times 2 bay floor system from building A at $\Delta = 474$ mm (ultimate static capacity) and (b) 4 bay \times 4 bay floor system from building A at $\Delta = 497$ mm

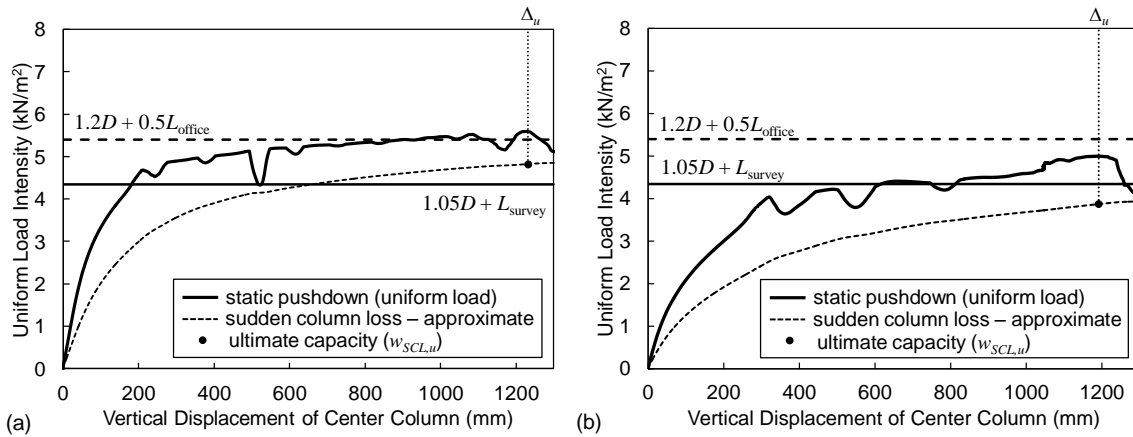


Fig. 15. Load-displacement curves under near-penultimate column loss: (a) 4 bay \times 4 bay floor system from building A; (b) for 3 bay \times 4 bay floor system from building B

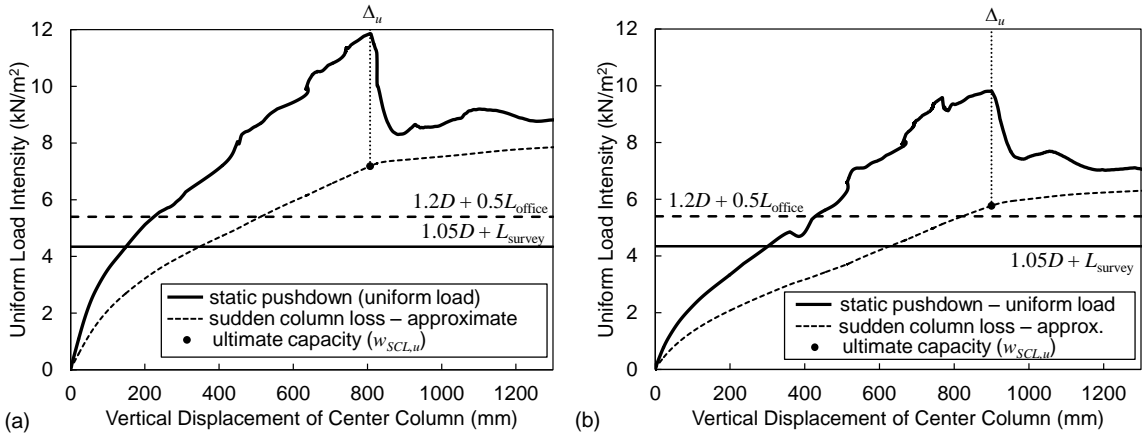


Fig. 16. Load-displacement curves under near-penultimate column loss for floor systems with horizontal ties that satisfy UFC 4-023-03: (a) 4 bay × 4 bay system from building A; (b) 3 bay × 4 bay system from building B

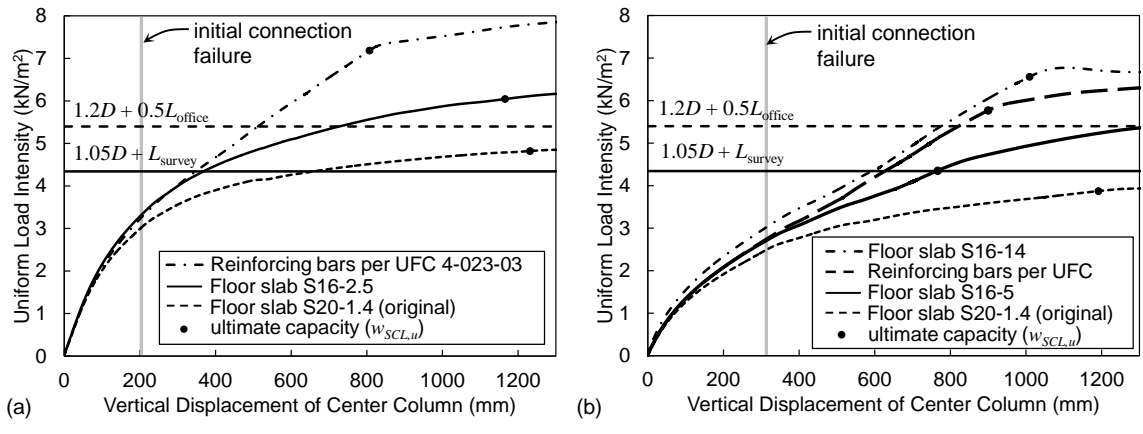


Fig. 17. Load-displacement curves for floor systems with different levels of slab reinforcement under sudden loss of near-penultimate columns: (a) 4 bay × 4 bay system from building A; (b) 3 bay × 4 bay system from building B

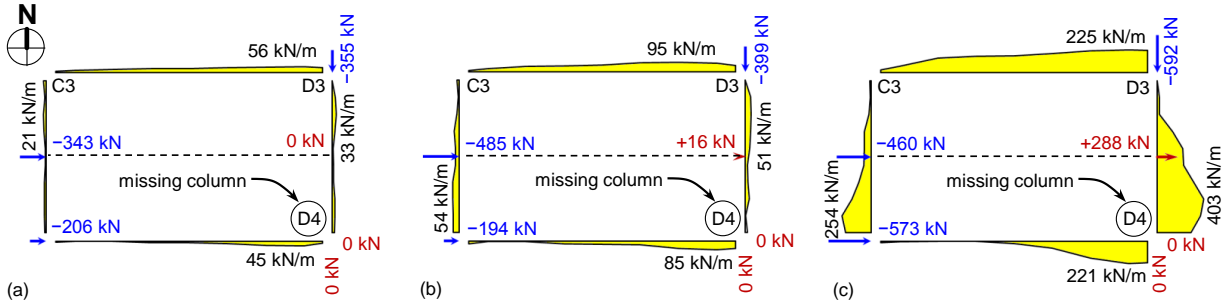


Fig. 18. Axial forces at beam ends (arrows) and tensile force per length normal to slab edges (filled areas) at ultimate static load for 4 bay \times 4 bay floor system from building A under loss of near-penultimate column (D4): (a) floor slab S20-1.4; (b) floor slab S16-2.5; (c) floor slab S20-1.4 with reinforcing bars that satisfy UFC 4-023-03

tie force requirements

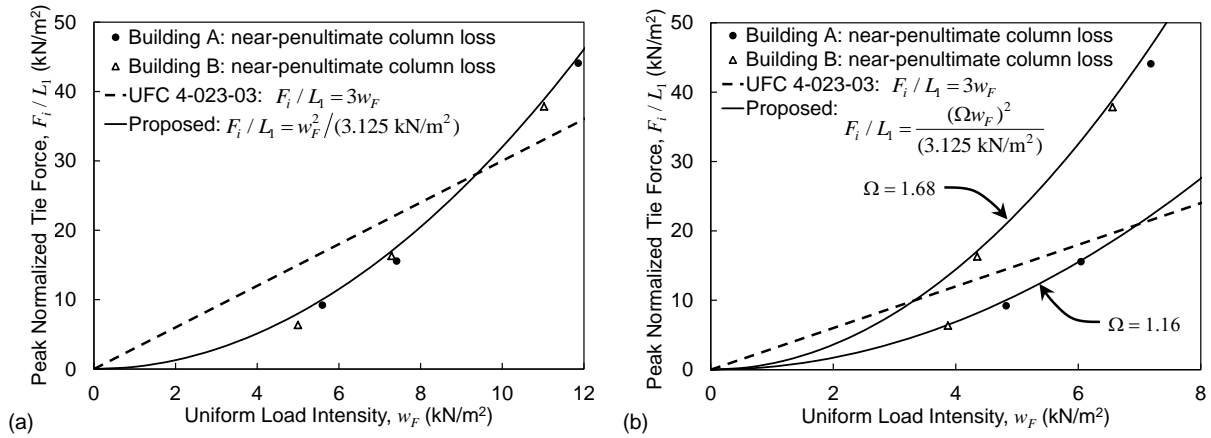


Fig. 19. Relationships between normalized tie forces in slab and uniform floor load intensity:

(a) quasi-static loading; (b) sudden column loss